

Article

A Predictive Energy Management Strategy for Heavy Hybrid Electric Vehicles Based on Adaptive Network-Based Fuzzy Inference System-Optimized Time Horizon

Benxiang Lin ^{1,2} , Chao Wei ^{1,2,*}, Fuyong Feng ^{1,2} and Tao Liu ³

¹ School of Mechanical Engineering, Beijing Institute of Technology, Beijing 100081, China; linbenxiang@126.com (B.L.); ffymieluo@126.com (F.F.)

² National Key Laboratory of Special Vehicle Design and Manufacturing Integration Technology, Beijing 100081, China

³ Inner Mongolia First Machinery Group Co., Ltd., Baotou 014030, China; liutao02508@163.com

* Correspondence: weichaobit@163.com

Abstract: Energy management strategies play a crucial role in enhancing the fuel efficiency of hybrid electric vehicles (HEVs) and mitigating greenhouse gas emissions. For the current commonly used time horizon optimization methods that only target the trend curve of the optimal battery state of charge (SOC) trajectory obtained offline, which are only suitable for buses with known future driving conditions, this paper proposed an energy management strategy based on an adaptive network-based fuzzy inference system (ANFIS) that optimizes the time horizon length and enhances adaptability to driving conditions by integrating historical vehicle velocity, accelerations, and battery SOC trajectory. First, the vehicle velocity prediction model based on the radial basis function (RBF) neural network is used to predict the future velocity sequence. After that, ANFIS was used to optimize and update the length of the forecast time horizon based on the historical vehicle velocity sequence. Finally, compared with the fixed time horizon energy management strategy, which is based on model predictive control (MPC), the average calculation time of the energy management strategy is reduced by about 23.5%, and the fuel consumption per 100 km is reduced by about 6.12%.

Keywords: energy management strategy (EMS); model predictive control (MPC); adaptive network-based fuzzy inference systems (ANFIS); hybrid electric vehicle (HEV)



Citation: Lin, B.; Wei, C.; Feng, F.; Liu, T. A Predictive Energy Management Strategy for Heavy Hybrid Electric Vehicles Based on Adaptive Network-Based Fuzzy Inference System-Optimized Time Horizon. *Energies* **2024**, *17*, 2288. <https://doi.org/10.3390/en17102288>

Academic Editor: Ahmed Abu-Siada

Received: 9 April 2024

Revised: 7 May 2024

Accepted: 8 May 2024

Published: 9 May 2024



Copyright: © 2024 by the authors. Licensee MDPI, Basel, Switzerland. This article is an open access article distributed under the terms and conditions of the Creative Commons Attribution (CC BY) license (<https://creativecommons.org/licenses/by/4.0/>).

1. Introduction

With the escalating global environmental challenges, governments worldwide are increasingly adopting stringent measures to curb carbon emissions, leading to a growing trend of electrifying heavy vehicles. As an intermediate solution, range-extended hybrid power technology not only addresses the limited driving distance issue of heavy vehicles but also significantly mitigates carbon emissions in line with governmental environmental protection requirements. Moreover, it offers potential cost reductions that align with consumer demands. Consequently, enhancing the energy efficiency and dynamic response time of electric power in heavy hybrid electric vehicles (HEVs) has become paramount.

Energy management strategy is the focus and difficulty of research in the field of hybrid electric vehicles, is the core technology of hybrid electric vehicles that directly determines the fuel economy, power, and drivability of the vehicle, and is of great significance for improving the economy and efficiency of the vehicle. The main task of energy management is to achieve the optimal distribution of power source or torque under the premise of satisfying the driver's power demand to optimize the vehicle performance. The different control strategies proposed in the existing literature are all aimed at achieving one or more optimal goals, which mainly include optimal fuel economy, lowest emission, lowest system cost, and best vehicle performance. Yang et al. [1] proposed a rolling convergent

equivalent consumption minimization strategy (ECMS) for the energy management of PHEV under two real-world driving cycles; the optimized energy management strategy improved fuel economy by 3.7% and 5.2%, respectively, over PHEVs using traditional energy management strategies. Tang et al. [2] proposed a predictive energy management strategy considering PHEV driving route information. The results demonstrate that the proposed model predictive control (MPC) approach yields a significant reduction in total cost, achieving a decrease of 21.1% compared to the CD-CS method. Additionally, the implementation of the performance measurement program (PMP) method only leads to a marginal increase in total cost by 2.3%. In addition, in Refs. [3–7], the impact of energy management strategies on the energy utilization rate of HEVs has been discussed in detail, so the optimization of energy management strategies is the main method for improving the energy utilization rate of hybrid power system for HEVs.

At present, there are two main categories of energy management strategies, the rule-based (RB) energy management strategy [8–10] and optimization-based EMS [11–13]. Early energy management methods adopted control methods based on clear rules [10,14] and fuzzy control algorithms based on fuzzy rules [15–17]. Later, control methods based on global optimization were widely used, such as the dynamic programming (DP) energy management algorithm [18–20] and the genetic algorithm (GA) [21–23]. However, the real-time performance of global optimization algorithms is poor, and it is only applicable to vehicles with known future working conditions, such as HEV buses. In recent years, with the emergence of various advanced intelligent energy management methods, representative methods have included an equivalent fuel consumption control algorithm (ECMS) based on instantaneous optimization [24–26], local optimization algorithms, such as the model predictive control (MPC) algorithm [27–29], etc. In the abovementioned optimization-based energy management methods, MPC, which takes into account both local optimal and real-time performance, has attracted attention and has been widely used in the research of energy management strategies.

MPC is based on different prediction models and adopts the rolling horizon optimization principle. It has the advantages of strong robustness, good control effect and high stability and has been widely used in linear and nonlinear control systems. Hao et al. [30] optimized the predictive model, combining driving intention recognition and driving condition prediction with MPC, with the goal of improving fuel consumption while maintaining the SOC of the battery. To further improve the calculation efficiency, the model was discretized and linearized, and the MPC problem was transformed into a quadratic programming problem, which can be effectively solved using the interior point method. Compared with the rule-based method, the predictive control strategy successfully improved the fuel economy of hybrid electric vehicles. Xiang et al. [31] optimized the prediction model and proposed a vehicle speed predictor based on radial basis function (RBF) neural network, which is used to predict short-term vehicle speed and has the advantages of fast convergence and low computational complexity. Then, energy management is regarded as a nonlinear constrained optimization problem, which is solved by nonlinear MPC. Kohut et al. [32] used the prediction model of integrated traffic data to obtain real-time traffic information from an intelligent traffic system (ITS) and predicted vehicle velocity by considering the influence of traffic density. Yu et al. [33] proposed an energy-saving predictive control strategy considering traffic signal light information and used two model predictive controller switching strategies to solve the problem of traffic signal light information model discontinuity, which can significantly improve the fuel economy of vehicles. Shu et al. [34] applied DP to MPC architecture; with an increase in the predicted line-of-sight, the calculation time increased rapidly, and the equivalent fuel consumption gradually decreased. Zhang et al. [35] adopted the Pontryagin maximum principle (PMP) in the role of rolling optimization and developed the MPC real-time optimization energy management strategy based on PMP; the advantage of this method is that the calculation time for updating control input is basically constant, but the disadvantage is that the differential equation obtained using the continuous method must be discretized in the time

domain, and the algorithm may fail due to the discretization error. The abovementioned studies assume that future driving conditions have been determined, but the velocity of the vehicle is constantly changing during the actual driving process, so the electric power required by the HEVs for future driving is also uncertain. In addition, some scholars combined robust control with MPC for the non-deficiency of the electric power demand side, and verified the effectiveness of the method through simulation; due to the dynamic changes in driving environment and driving conditions, the system's constraints (such as driving style) are also randomly changing, especially for complex nonlinear systems. How to effectively describe random constraints and implement real-time optimization control is a challenge. Robust MPC is not yet suitable for HEV energy management strategies in complex driving conditions [36].

Therefore, combining vehicle velocity prediction with MPC can be a way to optimize the energy management strategy for HEVs [37–41]. In ref. [42], the research shows that the combination of energy management strategy and vehicle velocity prediction can greatly improve the real-time performance and fuel economy of energy management strategy and improve the working condition adaptability of energy management strategy. With the rapid development of reinforcement learning (RL) algorithms, Chen et al. combined vehicle velocity prediction with MPC to build an Elman neural network velocity predictor with multiple feature inputs. They also used the double Q-learning (DQL) algorithm to optimize the allocation of battery output power [43]; however, when the vehicle velocity suddenly changes, the predicted future vehicle velocity deviates significantly from the actual future vehicle velocity, and the power output of the battery optimized by DQL may not be optimal. However, the abovementioned MPC methods all assume a constant prediction time horizon. Cao et al. proposed a method to control the accuracy of vehicle speed prediction by changing the prediction time scale and constructing a real-time prediction model with variable levels. The experiment verifies the correctness of the strategy, and the fuel economy of the vehicle is greatly improved compared with the traditional fixed line-of-sight MPC [44]. If the prediction time domain is set short, it can reduce the amount of calculation and make it easy to achieve real-time control, but it may lead to poor control results and cannot approach the optimal results. If the prediction time domain is set long, the number of calculations is too large, which is not conducive to real-time control. Therefore, selecting an appropriate prediction time domain length is crucial to the performance of MPC. For the current commonly used time horizon optimization methods that only target the trend curve of the optimal battery state of charge (SOC) trajectory obtained offline, which are only suitable for buses with known future driving conditions [45], this paper proposed an energy management strategy based on an adaptive network-based fuzzy inference system (ANFIS) that optimizes the time horizon length and enhances adaptability to driving conditions by integrating historical vehicle velocity, accelerations, and battery SOC trajectory. ANFIS has both the advantages and characteristics of the strong learning ability of neural networks and the advantages of a fuzzy logic system that makes it easy to absorb expert and empirical knowledge. It can effectively solve highly nonlinear problems and has good robustness and high accuracy [24].

The major contributions of this paper are the following:

1. To further optimize the predictive energy management strategy and improve the fuel economy of HEVs, a predictive energy management strategy based on ANFIS optimization was proposed.
2. The RBF neural network is applied to predict vehicle velocity in MPC, aiming at optimal fuel consumption; DP is used to solve the optimal diesel genset output power in the forecast time domain.
3. The performance is verified through comparison among different methods.

The rest of this paper is organized as follows. Section 2 describes the plant model of HEVs. In Section 3, the ANFIS method is provided with a detailed description of how to optimize the time horizon and use it in an energy management strategy based on MPC.

Section 4 provides simulation verification for the proposed method, and Section 5 draws the main conclusion.

2. The Plant Model of HEV

The topology of the distributed independent electric drive-heavy HEV is shown in Figure 1, and the power source is composed of two parts, a lithium-ion power battery pack and a diesel genset. The diesel genset consists of a generator rated at 150 kW with a peak of 260 kW and a diesel engine with a displacement of 12 L. The distributed independent electric drive is composed of six hub motors, with the specific parameters presented in Table 1.

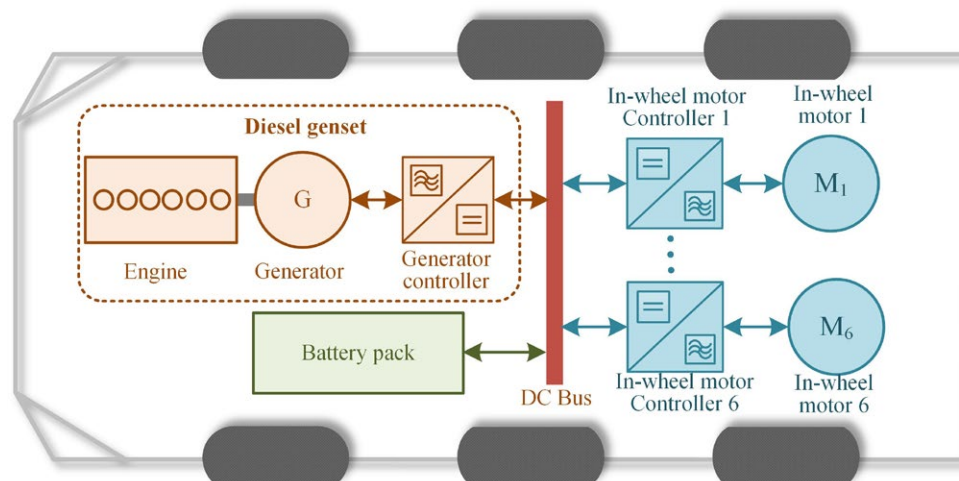


Figure 1. Configuration for hybrid electric vehicles.

Table 1. Basic parameters of the HEV.

Component	Item	Value
Vehicle	Curb weight (kg)	16,000
	Wheel radius (m)	0.56
	Wind area (m ²)	3.2
	Coefficient of rolling resistance	0.008
	Air drag coefficient	0.35
	Gravity acceleration (m/s ²)	9.8
Diesel genset	Peak power (kW)	260
	Rated power (kW)	150
	Engine rotational inertia (kg·m ²)	92.77
	Generator rotational inertia (kg·m ²)	3.297
Hub motor	Peak power (kW)	66
	Rated power (kW)	46
	Maximum speed (rpm)	5000
	Peak torque (Nm)	1750
	Rated torque (Nm)	1200
Battery	Type	Lithium battery
	Capacity (Ah)	75
	Rate Voltage (V)	601.2
Hub motor transmission	Gear Ratio	7.885
Hub motor controller	Efficiency (%)	90

2.1. Vehicle Dynamics

According to the vehicle power balance formula, the dynamic formula of the range-extended hybrid vehicle is expressed as follows [46]:

$$F_{\text{trac}} = f_g m_{\text{car}} g \cos \theta + \frac{\rho A_f C_d v_{\text{car}}^2}{2} + m_{\text{car}} g \sin \theta + \delta m \frac{dv_{\text{car}}}{dt} \quad (1)$$

where F_{trac} is the vehicle driving force, f_g is the coefficient of rolling resistance, m_{car} is the vehicle mass, v_{car} is the vehicle velocity, g , θ , A_f , and C_d represent gravity acceleration, road slope, wind area, and air drag coefficient, and ρ is the density of the air. The relationship between wheel speed and wheel torque is expressed as follows [46]:

$$\begin{cases} T_{\text{wheel}} = F_{\text{trac}} \cdot r_{\text{wheel}} \\ n_{\text{wheel}} = \frac{v_{\text{pre}}}{r_{\text{wheel}}} \end{cases} \quad (2)$$

where T_{wheel} is the driving moment at the center of the vehicle's driving wheel, and r_{wheel} is the wheel radius.

The total power balance equation is given as follows [46]:

$$P_{\text{req}} = \frac{F_{\text{trac}} \cdot v_{\text{car}}}{\eta_m \cdot \eta_{\text{tran}}} = P_{\text{bat}} + P_g \quad (3)$$

where P_{req} is the vehicle demand power, η_m is the efficiency of the hub motor, η_{tran} is the efficiency of the hub motor transmission (90%) with the driving moment at the center of the vehicle's driving wheel, and r_{wheel} is the wheel radius.

2.2. Diesel Genset Model

The output shaft of the engine is rigidly connected with the input shaft of the generator, and the speeds of the two are equal. Considering the rotational inertia of the engine and the generator, the speed, torque, and output power of the engine and the generator meet the following requirements [47]:

$$\begin{cases} \dot{m}_{\text{fuel}} = f(n_e, T_e) \\ P_g = \frac{T_g \cdot n_g}{\eta_g \cdot 9550} \\ T_e - T_g = (J_e + J_g) \frac{\pi}{30} \frac{dn_e}{dt} \\ n_g = n_e \end{cases} \quad (4)$$

where \dot{m}_{fuel} is the engine fuel consumption rate, n_e is the engine speed, T_e is the engine torque, T_g is the generator torque, P_g is the generator output power, η_g is the generator efficiency, J_g is the generator rotational inertia, and J_e is the engine rotational inertia.

A brake-specific fuel consumption (BFSC) map of the engine is shown in Figure 2. The generator efficiency diagram is shown in Figure 3.

According to Figure 2, we can find out the corresponding fuel consumption of the engine under different speeds and torques to calculate the fuel consumption. According to Figure 3, we can find out the generator efficiency corresponding to the different speeds and torques of the generator.

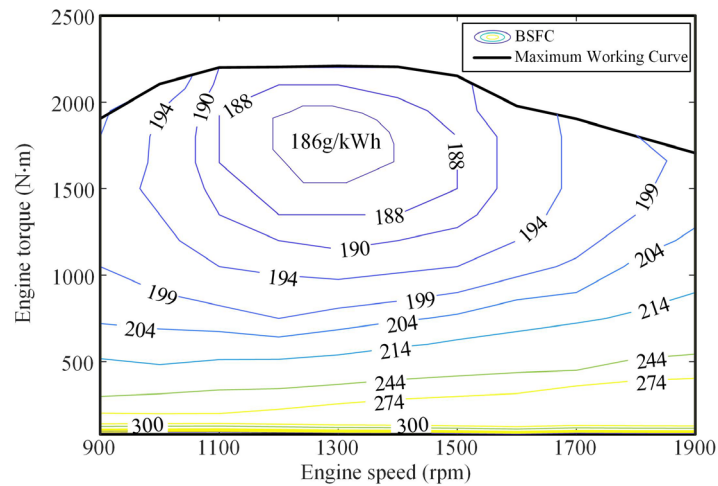


Figure 2. BSFC map of the diesel engine.

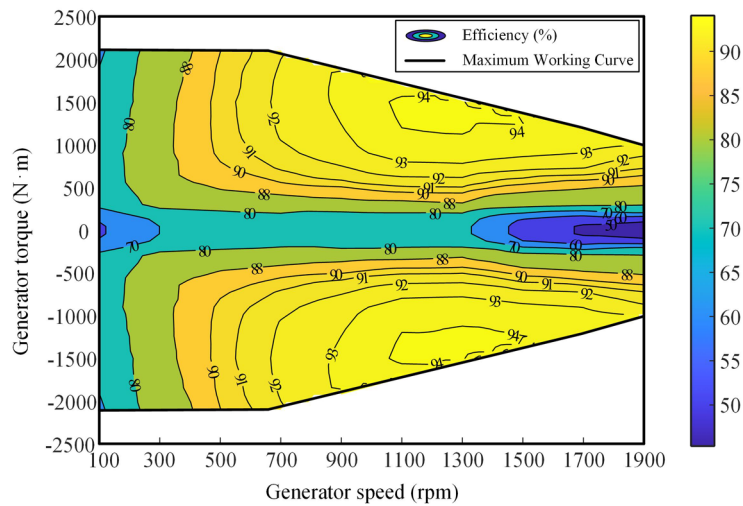


Figure 3. The generator efficiency map.

2.3. Battery Model

As the second electric power source of the vehicle, the power battery is used to adjust the balance of the front and rear power chains in the energy management strategy, which can not only make up for the problem of insufficient power caused by the sluggish response of the engine but also recycle braking energy and improve the energy utilization rate. Because of the advantages of high power density and high charge–discharge efficiency, a power battery cell is selected in this paper, and the power battery pack is equivalent to a circuit composed of a voltage source and a battery internal resistance in series.

This paper does not consider the impact of temperature on the battery’s state of charge (SOC) and internal resistance. According to the battery equivalent circuit diagram, the relationship between the battery current and the output power in the circuit is formulated as follows [24]:

$$\begin{cases} P_{bat} = E_{bat}i_{bat} - R_{bat}i_{bat}^2 \\ i_{bat} = \frac{E_{bat}}{2R_{bat}} - \sqrt{\left(\frac{E_{bat}}{2R_{bat}}\right)^2 - \frac{P_{bat}}{R_{bat}}} \\ U_{bat} = E_{bat} - R_{bat}i_{bat} \end{cases} \quad (5)$$

where P_{bat} is the battery output power, E_{bat} is the open-circuit voltage of the battery, i_{bat} is the battery output current, R_{bat} is the internal battery resistance, and U_{bat} is the battery terminal voltage.

The relationship between the battery open-circuit voltage and the SOC of the power battery can be obtained using the table. The relationship between the battery open-circuit voltage and the SOC of the power battery in the battery charging mode and the battery discharging mode is shown in Figure 4.

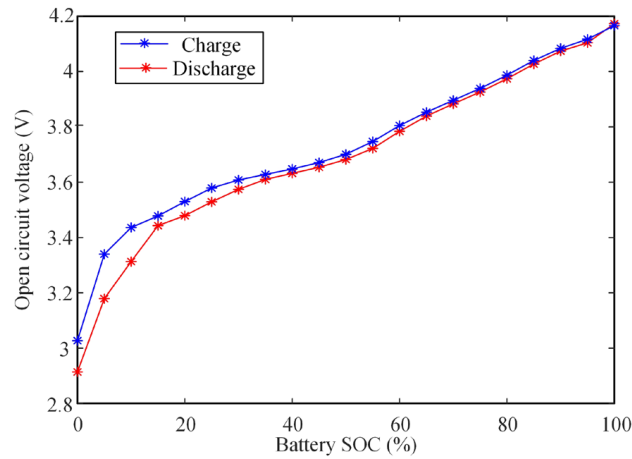


Figure 4. Open-circuit voltage of the battery cell.

The calculation of the power battery SOC is obtained using the ratio of residual capacity to total capacity, expressed as follows [24]:

$$\begin{cases} SOC_{bat} = \frac{Q_{bat_max} - Q_{bat_used}}{Q_{bat_max}} \\ Q_{bat_used} = (1 - SOC_{bat_initial}) + \int_0^{\Delta t} i_{bat} dt \end{cases} \quad (6)$$

where SOC_{bat} is the battery SOC, Q_{bat_max} is the maximum battery capacity, Q_{bat_used} is the power consumption of the battery, and $SOC_{bat_initial}$ is the initial SOC of the battery.

2.4. Hub Motor Model

The establishment of the hub motor model is similar to that of the engine and generator, that is, the electromagnetic and thermal effects of the motor are ignored, and the test modeling method is also adopted to model the motor by obtaining the steady-state test data of the motor. Figure 5 shows the external characteristics and efficiency diagram of the hub motor.

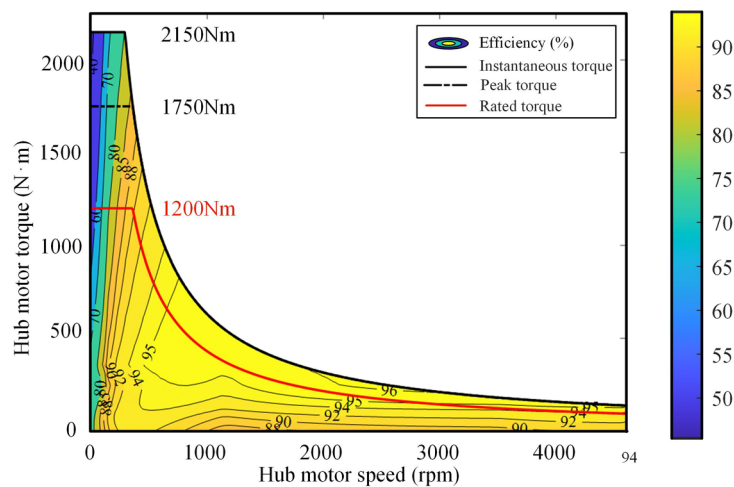


Figure 5. Hub motor efficiency map.

The working efficiency of the wheel motor is obtained using steady-state test data and can be expressed by the formula as follows [24]:

$$\eta_m = f(T_m, n_m) \tag{7}$$

where, η_m is the working efficiency of the hub motor, and T_m and n_m are the torque and speed of the hub motor, respectively.

The output power formula of the hub motor is expressed as follows [24]:

$$p_m = \frac{T_m \cdot n_m}{9550 \cdot \eta_m} \tag{8}$$

3. Architecture of Control System

The energy management strategy with MPC for time horizon length optimization based on ANFIS is shown in Figure 6.

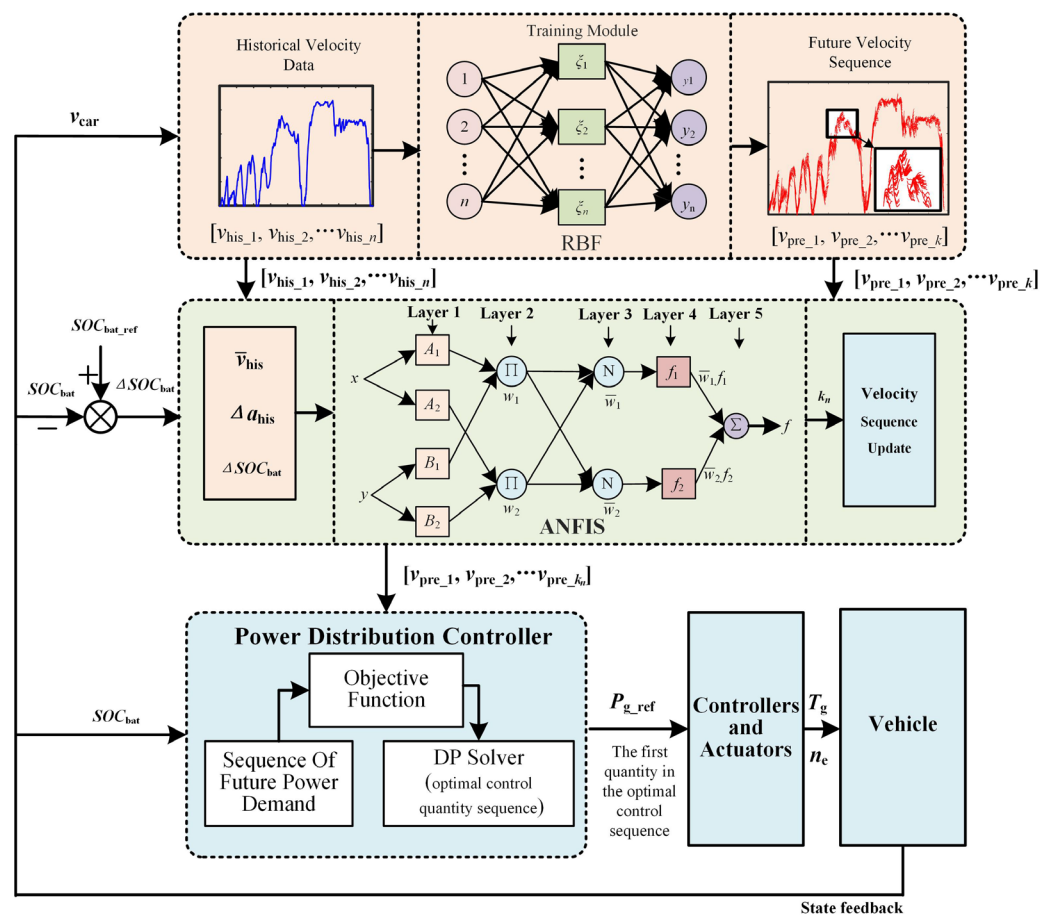


Figure 6. Architecture of control system.

First, through the vehicle velocity prediction model based on RBF, the historical speed is used to predict the velocity sequence in the future period of time. At the same time, according to the historical vehicle velocity sequence, the average vehicle velocity, the difference between maximum acceleration and minimum acceleration, and the deviation between the current SOC_{bat} and the reference trajectory SOC_{bat_ref} can be obtained in the past period of time. The abovementioned parameters are taken as input values of the ANFIS controller, and the prediction time domain of the current moment can be obtained through the rules formulated using ANFIS. The time horizon length of the predicted future velocity sequence is updated, and a future velocity sequence that is more suitable for the current driving condition is obtained. Then, the power distribution controller obtains the

future power demand sequence by updating the predicted velocity sequence. Then, to optimize the fuel economy, the future diesel genset control quantity sequence is obtained through a DP solution, and the first control quantity in the future control quantity sequence is taken as the target quantity of the bottom actuator. Finally, the vehicle model state variables are fed back to the power distribution and ANFIS controllers.

3.1. Prediction Model

Vehicle velocity prediction is a typical nonlinear time series prediction problem. The radial basis function neural network has obvious advantages in solving this kind of prediction problem. In this paper, the vehicle velocity prediction model is established by using the RBF neural network.

The RBF neural network is classified as a static neural network, which represents a static mapping relationship between input and output. To apply the theory of the RBF neural network to the vehicle velocity prediction model, it is crucial to determine the model's input and output variables. In vehicle velocity prediction, factors such as time, weather conditions, and traffic information may play significant roles in influencing future vehicle velocity. However, obtaining and integrating these data with current vehicle velocity information can be challenging. Conventional vehicle velocity prediction models often combine acceleration prediction with vehicle velocity prediction to make accurate forecasts because acceleration reflects changes in velocity and serves as an indicator of driving conditions. Neural networks possess learning and fitting capabilities that enable them to effectively incorporate acceleration into the process of understanding and adapting to various driving conditions. The process of vehicle velocity prediction model based on RBF is shown in Figure 7.

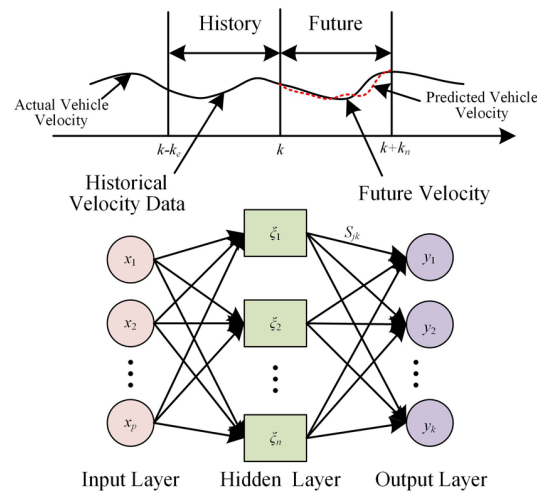


Figure 7. Flowchart of vehicle velocity prediction based on RBF.

This paper adopts the Gaussian activation function [48], so the Gaussian activation function is defined as follows:

$$\zeta_\alpha = \exp\left(-\frac{1}{2\sigma^2} \|x_m - c_i\|^2\right), (\alpha = 1, 2, \dots, n) \tag{9}$$

In Formula (9), $\|x_m - c_i\|^2$ represents the Euclidean distance, c_i is the activation function center, and σ is the Gauss function of variance.

The output of the RBF layer is shown in the following formula [48]:

$$y_j = \sum_{i=1}^h s_{jk} \exp\left(-\frac{1}{2\sigma^2} \|x_m - c_i\|^2\right) \tag{10}$$

In Formula (10), $x_m = (x_p^1, x_p^2, \dots, x_p^n)$ represents the n th in the input sample vector, s_{jk} is the weight of the output point, and the formula of calculation is as follows [48]:

$$s_{jk} = \exp\left(-\frac{p}{c_{\max}^2} \|x_m - c_i\|^2\right) \tag{11}$$

where c_{\max} is the maximum.

Based on the above RBF neural network, a neural network computing model for fitting the future time series of vehicle velocity in the predicted time horizon can be established. The input parameters of this neural network consist of past vehicle velocity $[v_{\text{his}_1}, v_{\text{his}_2}, \dots, v_{\text{his}_n}]$, while the output parameters represent the predicted series of vehicle velocity within that specific time horizon $[v_{\text{pre}_1}, v_{\text{pre}_2}, \dots, v_{\text{pre}_k}]$.

3.2. Tables and Schemes B. Time Horizon Optimization Based on ANFIS

ANFIS is a fuzzy inference system based on the Takagi–Sugeno model. It realizes fuzzification, fuzzy inference, and the defuzzification of fuzzy control by neural networks. It adjusts fuzzy inference control rules using offline training and online learning algorithms, making the system develop itself toward self-adapting, self-organizing, and self-learning [49]. Due to its inherent simplicity and remarkable efficacy, it has found extensive applications in diverse real-world problem domains [24,50–52]. The basic structure of ANFIS is shown in Figure 8.

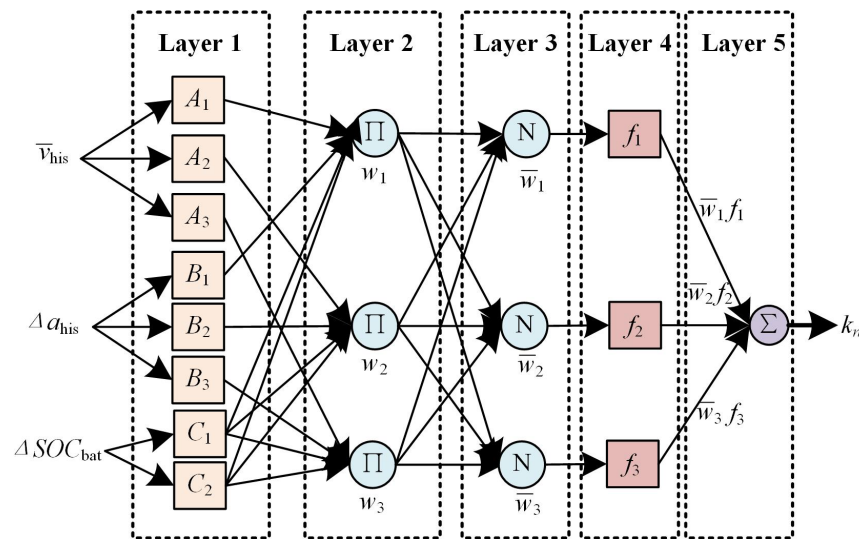


Figure 8. Basic structure of ANFIS.

3.2.1. Fuzzy Neural Network Structure

The ANFIS structural model has five layers [24]. For the convenience of introducing this network, $Q_{m,n}$ represents the output value of the n node in the m layer, and the value of m is 1 to 5.

The first layer consists of a fuzzy segmentation layer, in which the variable \bar{v}_{his} is represented by fuzzy sets A_1, A_2 , and A_3 , and the variable Δa_{his} is represented by fuzzy sets B_1, B_2 , and B_3 . Similarly, the variable $\Delta \text{SOC}_{\text{bat}}$ is expressed using fuzzy sets C_1 and C_2 . Each fuzzy set is characterized by a node function, with the output of each node indicating the membership degree that signifies how well the input belongs to a specific fuzzy rule [24].

$$\begin{cases} Q_{1,i} = \mu_{A_i}(\bar{v}_{\text{his}}), i = 1, 2, 3 \\ Q_{1,j} = \mu_{B_j}(\Delta a_{\text{his}}), j = 1, 2, 3 \\ Q_{1,k} = \mu_{C_k}(\Delta \text{SOC}_{\text{bat}}), k = 1, 2 \end{cases} \tag{12}$$

where, $Q_{1,i}$, $Q_{1,j}$, and $Q_{1,k}$ are membership functions of fuzzy sets A_i , B_j , and C_k , respectively, and are expressed as follows using Gaussian functions:

$$\begin{cases} Q_{1,i} = \mu_{A_i}(\bar{v}_{\text{his}}), i = 1, 2, 3 \\ Q_{1,j} = \mu_{B_j}(\Delta a_{\text{his}}), j = 1, 2, 3 \\ Q_{1,k} = \mu_{C_k}(\Delta \text{SOC}_{\text{bat}}), k = 1, 2 \end{cases} \quad (13)$$

where parameters z and λ represent the center and width of the Gaussian function, respectively, serving as crucial precondition factors in our model.

The second layer is the rule inference layer, which is responsible for calculating the intensity of fuzzy rule excitation and multiplying it with the input signals to generate the corresponding output product. The mathematical expression can be formulated as follows:

$$Q_{2,i} = \omega_i = \mu_{A_i}(\bar{v}_{\text{his}})\mu_{B_j}(\Delta a_{\text{his}})\mu_{C_k}(\Delta \text{SOC}_{\text{bat}}) \quad (14)$$

The third layer is referred to as the fuzz layer, with the excitation intensity being standardized.

$$Q_{3,i} = \bar{\omega}_i = \frac{\omega_i}{\omega_1 + \omega_2 + \omega_3} \quad (15)$$

The fourth layer consists of adaptive nodes that function as the deblurring layer, with each node outputting an adaptive formula.

$$Q_{4,i} = \bar{\omega}_i f_i = \bar{\omega}_i(p_i \bar{v}_{\text{his}} + q_i \Delta a_{\text{his}} + r_i \Delta \text{SOC}_{\text{bat}} + n_i) \quad (16)$$

where, the parameters p_i , q_i , r_i , and n_i represent the variables in the latter part.

The fifth layer serves as the output layer, wherein the cumulative output of all input signals is computed, as depicted by the following expression:

$$Q_{5,i} = \sum_{i=1}^j \bar{\omega}_i f_i = \frac{\sum_i \omega_i f_i}{\sum_i \omega_i} \quad (17)$$

3.2.2. Learning Algorithms for Fuzzy Neural Networks

The fuzzy neural network system uses a BP backpropagation algorithm and the least squares method to complete the model of input/output data pairs. This method can extract the corresponding information (fuzzy rules) from the dataset, making the generated Takagi–Sugeno-type fuzzy inference system better at simulating the desired or actual input/output relationship. When the fuzzy neural system is learning, the learning error can be calculated according to the actual output value and the expected output value of the system, and then the system parameters can be adjusted through error backpropagation. The main adjusted system parameters are the weight ω , the center z of the Gaussian function, and the width λ . The learning error function is expressed as follows:

$$e = \frac{1}{2} \sum_{i=1}^j (f_i - f'_i)^2 \quad (18)$$

where, f_i and f'_i are the desired output and the actual output, respectively.

The adjustment method of parameters in the learning process is described in the following expression:

$$\begin{cases} \omega_{ij}(k+1) = \omega_{ij}(k) - \gamma \frac{\partial e}{\partial \omega_{ij}} \\ z_{ij}(k+1) = z_{ij}(k) - \gamma \frac{\partial e}{\partial z_{ij}} \\ \lambda_{ij}(k+1) = \lambda_{ij}(k) - \gamma \frac{\partial e}{\partial \lambda_{ij}} \end{cases} \quad (19)$$

where k is the number of iterations and $\gamma > 0$ is the learning rate.

3.2.3. Training Results

In this paper, the powerful self-organization, self-adaptation, and self-learning capabilities of ANFIS in function approximation are utilized to learn the optimal time horizon dataset of the dataset, as shown in Figure 9.

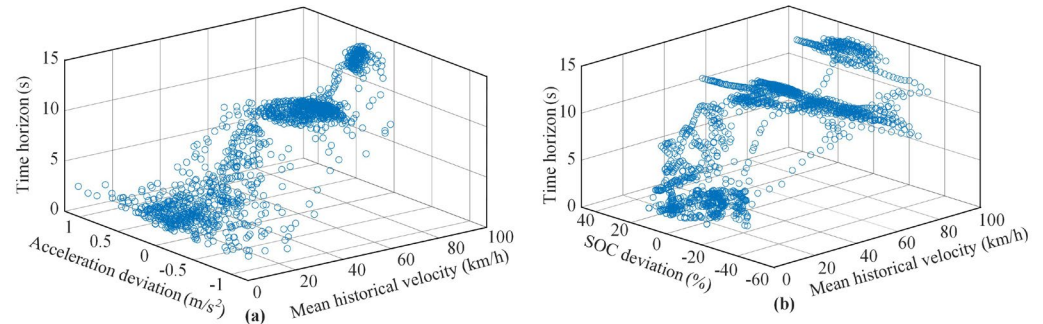


Figure 9. ANFIS training set. (a) Acceleration deviation and historical mean velocity with time horizon dataset; (b) SOC deviation and historical mean velocity vs. time horizon length dataset.

Because the backpropagation algorithm relies on the gradient information of each neuron's transfer function, excessively large inputs can result in extremely small gradients for the corresponding independent variables, hindering smooth weight and threshold adjustments. Therefore, prior to training, it is essential to normalize the input parameters to ensure convergence. Three input membership functions in the adaptive neural fuzzy system trained in this paper are all Gaussian functions, and the number of input membership functions is 3, 3, and 2, in turn, and the training times is 100. The ANFIS model structurally obtained after training is shown in the Figure 10, with the number of nodes being 58 and the number of fuzzy rules being 18.

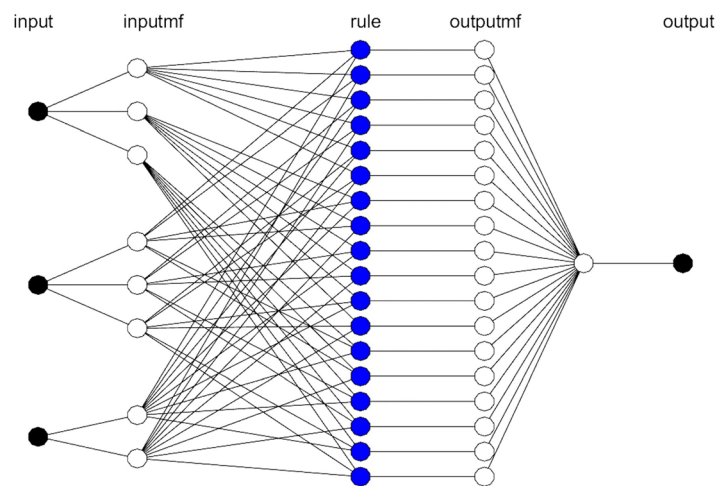


Figure 10. ANFIS model structural.

3.3. Cost Function and Limitations

The hybrid power system employs SOC maintenance mode. In this study, an ANFIS method is utilized to optimize the prediction time horizon and an MPC energy management strategy with fuel economy as the optimization objective is applied, solving it through dynamic programming (DP).

The DP algorithm is fundamentally a multi-stage decision-making optimization process, which is discretized into several stages in the time sequence, and each decision made in each stage leads to a corresponding state transition. Arranging the decisions made in

each stage in the time sequence ultimately forms the entire process's control sequence. Therefore, to apply the DP algorithm for global optimization, the system equation needs to be discretized. In this solution, one second is a stage, and the HEV is considered a whole system. The SOC_{bat} is considered the state variable, while engine speed n_e and generator torque T_g are regarded as control variables, resulting in the derivation of the following state transition equation:

$$\begin{cases} \dot{SOC}_{bat}(k+1) = SOC_{bat}(k) - \frac{E_{bat} - \sqrt{E_{bat}^2 - 4(P_{req}(k) - P_g(k))R_{bat}}}{2R_{bat}Q_{bat_max}} \\ u(k) = g(n_e(k), T_g(k)) \end{cases} \quad (20)$$

where $SOC_{bat}(k)$ is the state variable for stage k , $SOC_{bat}(k+1)$ is next phase of the system status, $u(k)$ is the k stage that controls the control variables of the diesel genset, g is the state transition function, P_{req} is the vehicle's required power, P_g is determined by the power of the diesel genset, and R_{bat} is the internal resistance of the battery. The principle of no aftereffect of the DP algorithm can also be verified from Equation (20), that is, the state of stage $k+1$ is only related to the state and control variables of stage k and is not related to the state of any previous stage.

The real-time optimization energy management of HEV is to optimize the optimization objective in the prediction time horizon at each sampling moment to obtain the optimal control sequence in the prediction time horizon, and only the first control quantity is used as the optimal control quantity at the current moment. Formulating a reasonable target cost function is the key to real-time optimization to achieve the optimal control effect. The primary goal of energy management is to reduce fuel consumption, so the cost function includes the fuel consumption of the engine. The battery of series HEV cannot be charged from the outside, and the electric energy fundamentally comes from the engine.

The battery is charged or discharged according to the driving demand, and the SOC_{bat} needs to be maintained within a certain range, so the cost function needs to limit SOC_{bat} . The solution of model predictive control is different from global optimization, which is to optimize the solution in the prediction time domain in the form of rolling optimization. The battery is in the state of charging or discharging at each moment, so this paper only penalizes the deviation of SOC_{bat} at the end of the prediction time horizon. In summary, the target cost function in the prediction time domain is as follows:

$$J = \int_k^{k+kn} m_{engine}(k) dt + \beta(SOC_{bat}(k+kn) - SOC_0) \quad (21)$$

where, kn represents the length of the forecast time domain, $SOC_{bat}(k+kn)$ represents the SOC_{bat} value at the end of the forecast time horizon, and SOC_0 is the reference SOC_{bat_ref} value. The second term in the formula is the terminal penalty term, which is used to penalize the ΔSOC at the end of the forecast time domain, and its weight coefficient is β .

When solving the transmission DP, this paper combines the idea of ECMS and optimizes it using the equivalent factor. Therefore, the product of penalty factor β and SOC_{bat} deviation and fuel consumption are not in the same dimension, and the electric energy is equivalent to fuel consumption through the equivalent conversion factor. Referring to the ECMS idea, the terminal electric energy consumption is converted into fuel consumption, and the terminal part of the cost function is improved as follows:

$$\begin{aligned} \beta(SOC_{bat}(k+kn) - SOC_0) &= f_{equ}(SOC_{bat}(k+kn) - SOC_{bat_ref}) \\ &= \frac{s_e}{Q_{fuel}} \left(\frac{E_{bat} Q_{bat_max} (SOC_{bat}(k+kn) - SOC_{bat_ref}) - (Q_{bat_max} (SOC_{bat}(k+kn) - SOC_{bat_ref}))^2 R_{bat}}{2} \right) \end{aligned} \quad (22)$$

where Q_{fuel} is the calorific value of fuel oil, S_e is the oil–electric conversion factor, and the formula incorporates the transformation of the SOC_{bat} deviation penalty in the predicted time horizon terminal into equivalent fuel consumption, which is denoted as f_{equ} .

Consequently, the optimal target cost function of the system can be reformulated as follows:

$$J = \int_k^{k+k_n} \dot{m}_{\text{engine}}(k) dt + f_{\text{equ}}(SOC_{\text{bat}}(k+k_n) - SOC_{\text{bat_ref}}) \quad (23)$$

If the f_{equ} is fixed, the driving condition adaptability is poor, resulting in continuous fluctuations in the SOC_{bat} when the vehicle is working. When the f_{equ} is small, the equivalent fuel consumption of the battery is relatively low, and the energy management system tends to use electricity, which easily leads to over discharge of the SOC_{bat} . On the contrary, when the f_{equ} is too large, the energy management system prefers oil, causing the SOC_{bat} to rise and deviate from the target value. To improve the fuel economy of tractors and maintain the stability of the SOC_{bat} , it is necessary to dynamically adjust the oil–electric equivalent factor to improve its adaptability. Through offline simulation, the relationship between the oil–electric conversion factor S_e and ΔSOC_{bat} is shown in the Figure 11.

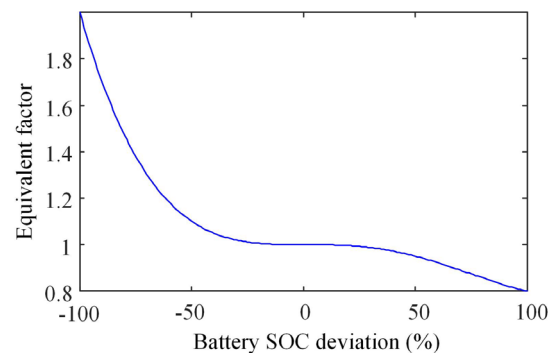


Figure 11. Curve of equivalent factor S_e and battery SOC deviation.

The inclusion of system constraints is imperative to ensure the safe and rational operation of both the diesel genset and battery. In the solution process, state variables, control variables, and output variables are discretized, leading to the formulation of the optimal problem as follows:

$$\begin{aligned} & \min_{u(k)} J(SOC(k), u(k)) \\ & \text{s.t.} \left\{ \begin{array}{l} SOC(k+1) = f(SOC(k), u(k)) \\ n_{e,\min} \leq n_e(k) \leq n_{e,\max}, T_{g,\min} \leq T_g(k) \leq T_{g,\max} \\ SOC_{\text{bat},\min} \leq SOC_{\text{bat}}(k) \leq SOC_{\text{bat},\max} \\ P_{\text{bat},\min} \leq P_{\text{bat}}(k) \leq P_{\text{bat},\max} \\ P_{e,\min} \leq P_e(k) \leq P_{e,\max} \end{array} \right. \quad (24) \end{aligned}$$

where $n_{e,\max}$ denotes the maximum value of engine speed, while $n_{e,\min}$ represents its minimum value. Similarly, $T_{g,\max}$ and $T_{g,\min}$ correspond to the maximum and minimum values of generator torque, respectively, whereas $P_{e,\max}$ and $P_{e,\min}$ signify the upper and lower bounds of diesel genset power, respectively.

3.4. Optimization Based on DP Algorithm

The forecasted vehicle velocity determines the power demand in the forecasted time horizon, and on this basis, a rolling optimization model is established by using DP.

The solution based on DP is shown in Figure 12. In each stage moment in the prediction time horizon, the system state variable SOC_{bat} is discretized, and the engine speed and torque are indirectly obtained by using the diesel genset power in the solution process. Starting from the terminal moment, the control quantity within the constraint range is traversed under the feasible state at each moment, the optimal solution and its control path are searched in reverse, and finally, the solution is searched forward.

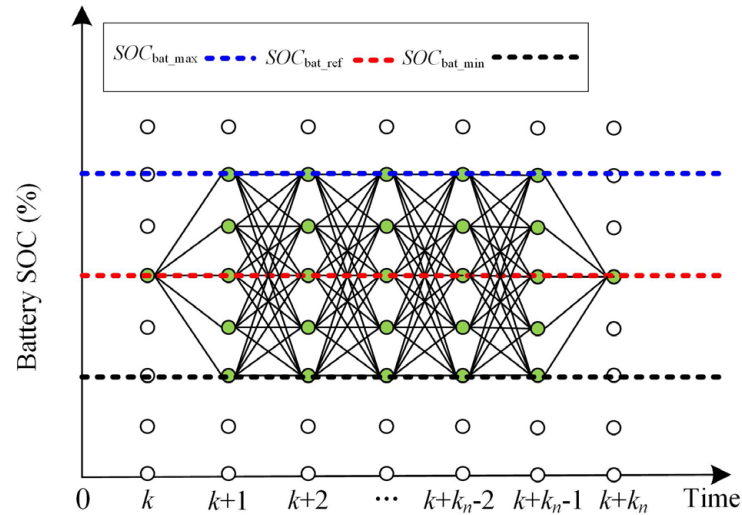


Figure 12. DP state and time discrete partition diagram.

When the DP algorithm is used for optimization, the terminal moment is different from the non-terminal moment. Because SOC_{bat} is constantly changing during vehicle driving, according to the cost function established by analysis in Section C, equivalent fuel consumption caused by SOC_{bat} change is not considered in the stage changes, except terminal moment, and only the terminal penalty term for SOC_{bat} deviation is added at the termination moment of the prediction time horizon.

When predicting the terminal in the time horizon, the cost function is as follows:

$$J_{k+k_n} = \min \{ L_{k+k_n}(SOC_{bat}(k+k_n), u(k+k_n)) + f_{equ}(SOC_{bat}(k+k_n) - SOC_{bat_ref}) \} \quad (25)$$

The state variable of the DP solving model is the SOC_{bat} , and the control variable is the generator torque and engine speed. The state of the system can be determined using the state variable SOC_{bat} and the diesel genset power. Discrete SOC_{bat} and diesel genset power, for each SOC_{bat} discrete value at time, traverse the diesel genset power that meets the constraint conditions and apply the corresponding optimal engine speed and generator torque to the system to obtain the SOC_{bat} at time. If the constraint range is not exceeded, the cost caused by the control quantity is calculated; otherwise, the control quantity is discarded. Starting from the prediction terminal, the optimal cost function of the state quantity that may be passed at each time is obtained, and it is iterated until the initial time to determine the optimal SOC_{bat} change sequence and control sequence in the prediction time horizon.

4. Simulation Results and Analysis

4.1. Training Setting

Given the variegated velocity of heavy-duty vehicles, which range from low to high, and the distinct urban conditions they operate in, it becomes imperative to develop a robust training set for the RBF neural network.

The information on five different cycles, including the Urban Dynamometer Driving Schedule (UDDS), New European Driving Cycle (NEDC), Highway Fuel Economy Test (HWFET), Supplemental Federal Test Procedure-US06 (SFTP-US06), and World Light

Vehicle Test Procedure (WLTP), is shown in Table 2. To validate the performance of the prediction model-based RBF in different cycles, five datasets of velocity profiles as sample cycle sets were combined into a training cycle set (UDDS–NEDC–HWFET–SFTP–US06–WLTP), as shown in Figure 13. Normalize the cycle datasets by transforming them into training data with a mean of zero and a standard deviation of one, and construct an RBF prediction model based on this normalized training data for predicting driving conditions. The China heavy-duty commercial vehicle test cycle-tractor trailer (CHTC-TT), as shown in Figure 14, was used to test the prediction model.

Table 2. Detailed cycle information of six different cycles.

Cycle	Velocity Max (km/h)	Average Velocity (km/h)	During Time (s)	Distance (km)
CHTC-TT	88	46.44	1800	21.3
UDDS	91.2	31.5	1370	12.07
NEDC	120	24.7	1180	11.02
HWFET	96.37	77.7	765	16.45
SFTP-US06	129.2	77.9	596	12.8
WLTP	131.3	46.5	1800	23.27

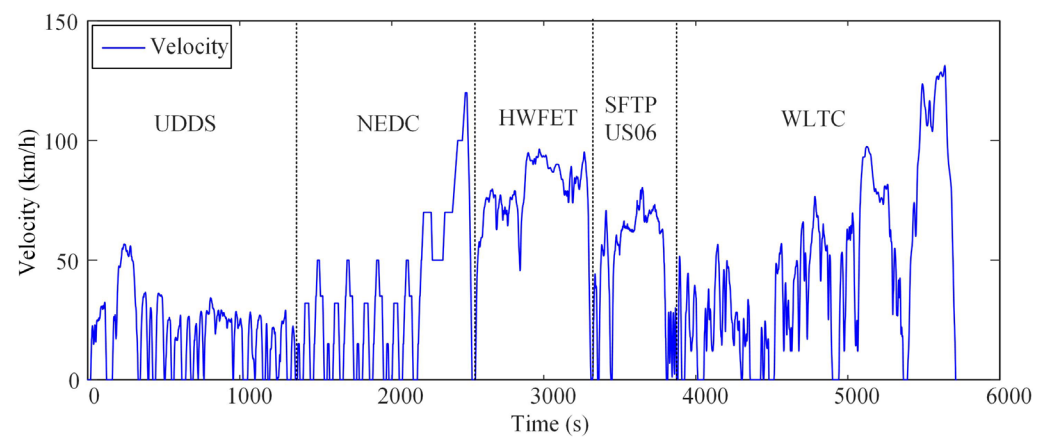


Figure 13. Sample vehicle velocity cycle datasets.

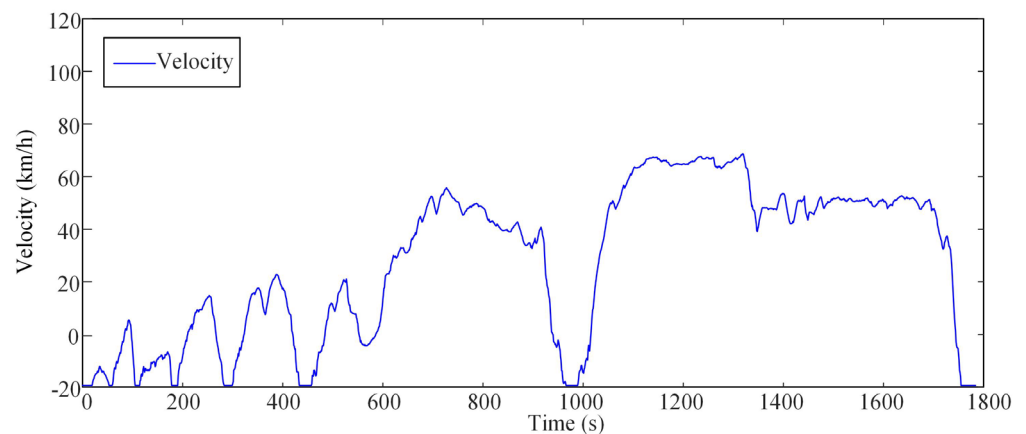


Figure 14. CHTC-TT-based test cycle set.

In this paper, the root mean square error is used as an indicator to evaluate the prediction accuracy, and the smaller the RMSE, the higher the prediction accuracy. The root mean square error is the square root of the ratio of the square sum of the deviation between

the observed value and the true value to the number of observations. It is commonly expressed as follows:

$$RMSE(k) = \sqrt{\frac{\sum_{i=1}^N (v_{pre}(k+i) - v_{car}(k+i))^2}{N}}, (i = 1, 2, \dots, N) \quad (26)$$

where $v_{pre}(k+i)$ and $v_{car}(k+i)$ are respectively the predicted value and true value of the vehicle velocity at the i time.

4.2. Simulation Analysis of RBF-MPC

In this section, the CHTC-TT cycle conditions were taken as an example, simulation experiments were conducted to study the effect of vehicle velocity prediction accuracy under the different time horizon lengths of vehicle velocity prediction, and the impact on the final energy consumption of the MPC energy management strategy was compared to improve the fuel economy of the energy management strategy. The simulation results and analysis are described below.

To study the influence of different prediction time horizon lengths on the velocity prediction effect, this section compares the simulation experiments of the RBF neural network velocity prediction model with the prediction time domain lengths of 5 s, 10 s, and 15 s respectively. Among these, the historical time horizon length is consistent with the prediction time horizon length, and the simulation results of the prediction accuracy are shown in Figure 15. As can be seen in Figure 15, when the vehicle velocity is low and the acceleration changes frequently, the predicted future vehicle velocity sequence has a large error; it also can be seen that with the extension of time in the prediction horizon, the vehicle velocity prediction error gradually increases, the vehicle velocity prediction error is more concentrated in acceleration sudden change, and the vehicle velocity prediction is more accurate in medium vehicle and high vehicle conditions.

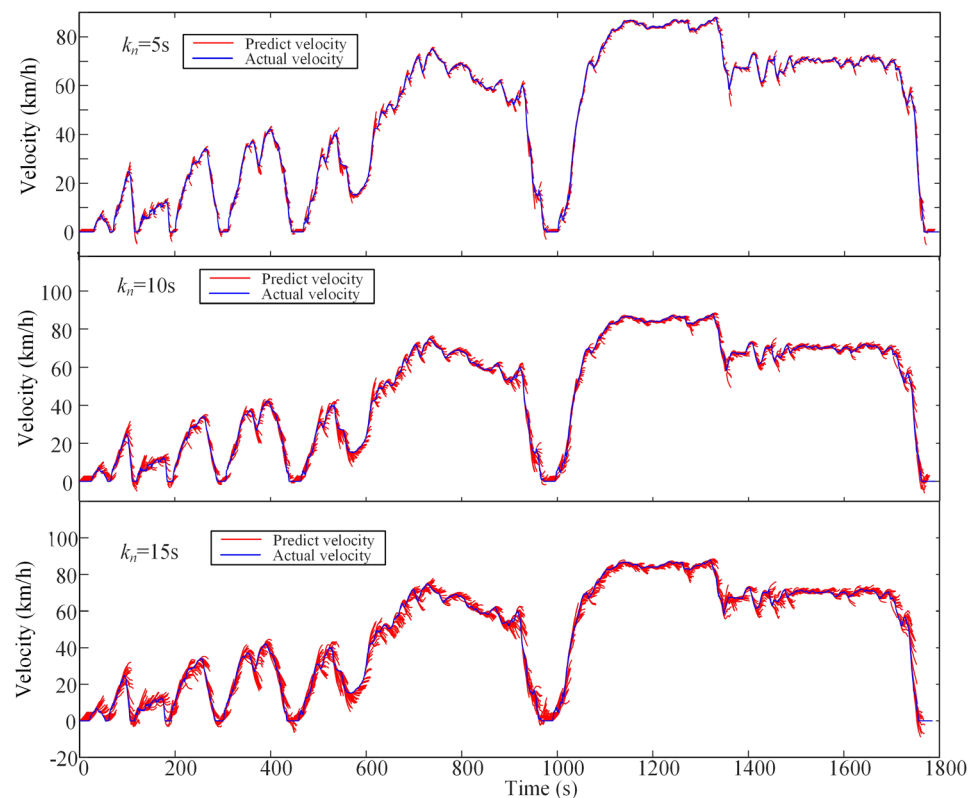


Figure 15. Velocity prediction results of different prediction time horizon lengths.

In addition, at 100–600 s, the vehicle velocity is low, the velocity is in a state of frequent change, and the acceleration change rate fluctuates greatly. Therefore, as shown in Figure 15, at 100–600 s, it is obvious that with an increase in the time horizon length, the deviation between the predicted vehicle velocity sequence and the future actual vehicle velocity sequence increases. When the velocity changes from large to small, the vehicle demand power decreases at this time. However, the error of the vehicle velocity prediction model will cause the predicted velocity to increase. The energy management strategy will plan the optimal output power of the diesel genset to meet the predicted vehicle demand power. In this way, the output power of the diesel genset will be greater than the actual demand power of the vehicle, so the electric power will be supplemented by the battery, resulting in an increase in SOC and fuel consumption.

At 1000–1600 s, when the vehicle velocity is high and the velocity state is stable, the fluctuation in the acceleration change rate is small. Therefore, as shown in Figure 15, with the increase in the time horizon length between 1000 and 1600 s, the predicted vehicle velocity sequence has a small deviation from the actual future velocity sequence. Even if the vehicle velocity fluctuates, the error of the vehicle velocity prediction model has no effect on the predicted velocity. At this time, the time horizon length increases, and the energy management strategy will solve the optimal output power of the diesel genset in the longer prediction time horizon length to achieve a better power output scheme and reduce fuel consumption.

The data in Figures 15–17 were counted, and Table 3 was obtained. As shown in Table 3, the prediction error of vehicle velocity and the corresponding simulation results of energy consumption under different prediction time horizons were counted. With an increase in the prediction time horizon, the prediction error of vehicle velocity also increases. When the prediction time horizon of vehicle velocity is extended from 5 s to 15 s, the prediction error of vehicle velocity is increased from 0.061 to 2.595. Therefore, considering the accuracy of vehicle velocity prediction, 5 s should be chosen as the optimal prediction time domain length.

However, from the perspective of vehicle energy efficiency, with an increase in the prediction time horizon, the MPC energy management strategy can obtain more adequate information on effective driving conditions, which is conducive to the improvement of the global optimization of the strategy, and the total vehicle fuel consumption is gradually reduced. As the vehicle velocity prediction time horizon length changes from 5 s to 15 s, vehicle fuel consumption is reduced from 17.85 to 17.16 L. In addition, due to the characteristics of model predictive control theory, the computational cost of energy management strategy also increases linearly with the increase in the prediction time horizon. Considering the real-time performance and fuel economy of the energy management strategy, 10 s is selected as the best predictive time domain length of RBF–MPC energy management strategy.

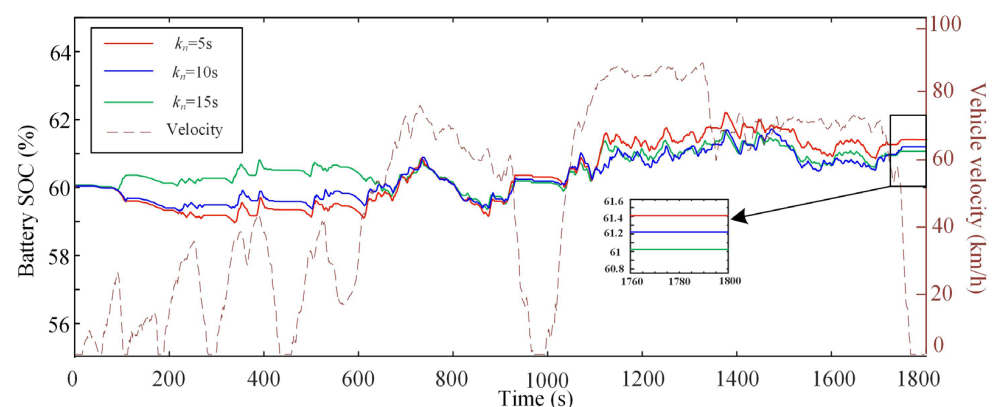


Figure 16. SOC trajectories for CHTC-TT driving cycle under different prediction time horizon lengths based on RBF–MPC.

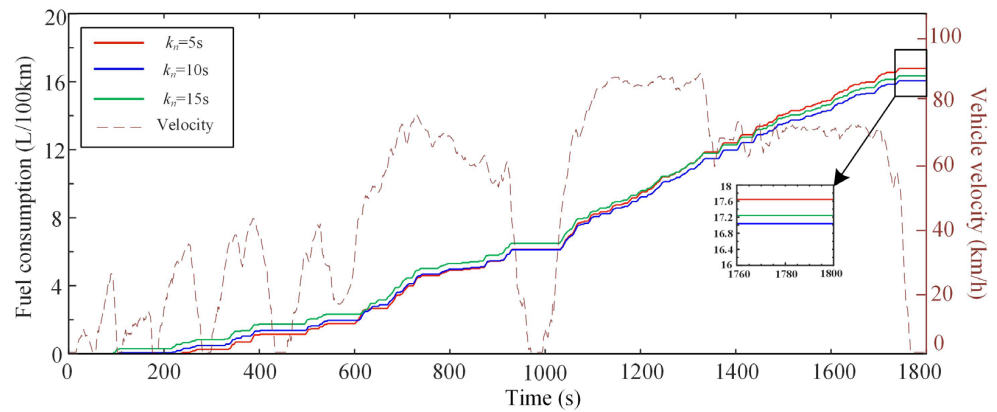


Figure 17. Fuel consumption curve for CHTC-TT driving cycle under different prediction time horizon length based on RBF-MPC.

Table 3. Comparison of vehicle velocity prediction and fuel consumption simulation results under different prediction time horizon lengths with RBF-MPC.

Time Horizon (s)	RMSE	Initial SOC	Final SOC	Fuel (L/100 km)	Calculation Time (s)
5	0.061	60	61.42	17.85	0.016
10	1.326	60	61.26	17.16	0.034
15	2.595	60	61.15	17.23	0.059

4.3. Simulation Analysis of RBF-ANFIS-MPC

To verify whether the energy management strategy based on MPC with an ANFIS-optimized time horizon established in this paper can more reasonably allocate the power of the engine-generator set and the battery and obtain better fuel economy compared with the energy management strategy based on RBF-MPC in a fixed time horizon, the CHTC-TT condition is selected for simulation. The simulation duration is 1800 s, with a time step of 0.01 s. The maximum time horizon is 15 s, while the fixed time horizon length is 10 s. The initial SOC is set to 60%, and the simulation results and analysis are described below.

The change in time horizon length is shown in Figure 18. The choice of time horizon length is crucial to update the predicted vehicle velocity sequence. As can be seen from Figure 18, the ANFIS controller designed in this paper has completed the time horizon length optimization. The ANFIS controller can output different time horizon length values according to different driving conditions. As can be seen in Figure 18, when the changes in history vehicle velocity and acceleration deviation were small, the time horizon length increased, and the maximum time domain length was 15 s. For comparison, the time horizon length of the energy management strategy with RBF-MPC is 10 s all the time.

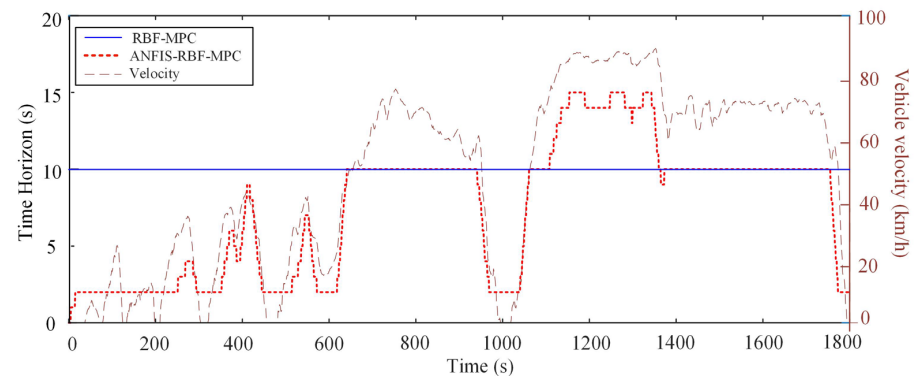


Figure 18. Comparison of time horizon lengths between the two methods.

Under the same input conditions, the same cost function and constraint conditions are adopted, and the SOC trajectory pairs of the MPC energy management strategy with a fixed time horizon length and an ANFIS-based variable time horizon MPC energy management strategy are shown in Figure 19. The fuel consumption is illustrated in Figure 20. The data in Figures 18 and 20 were counted, and Table 4 was obtained.

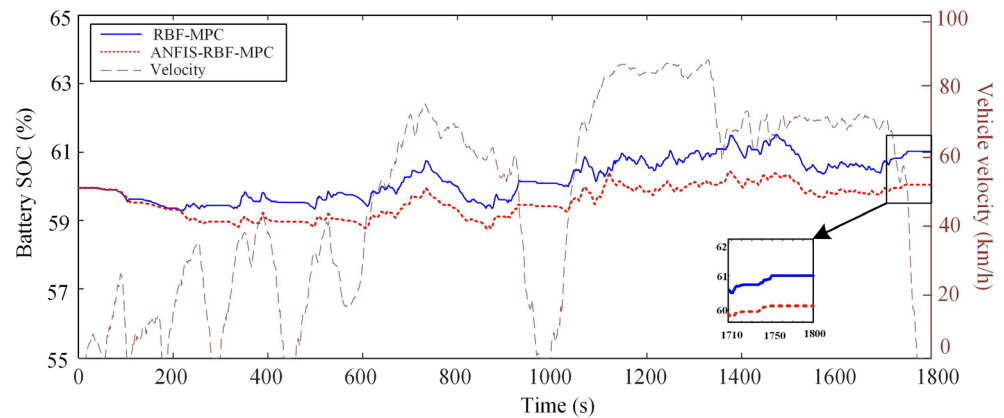


Figure 19. SOC trajectory of both strategies in the cycle.

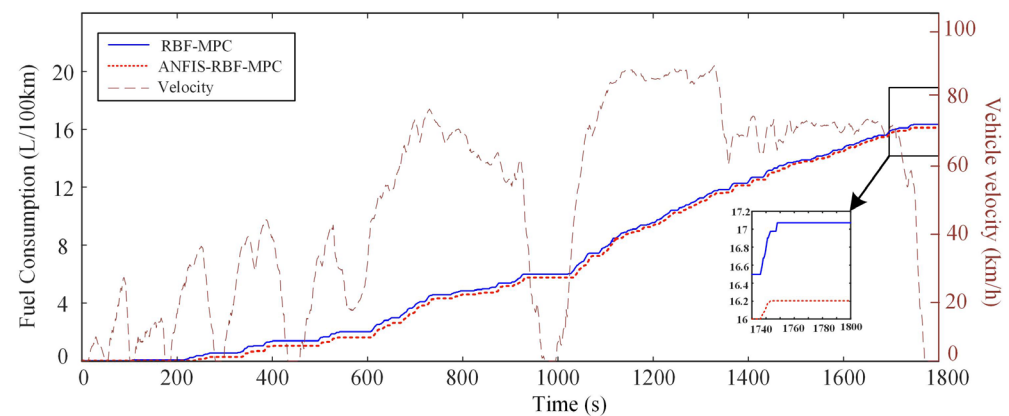


Figure 20. Temporal contrast in the horizon of time.

Table 4. Comparison of simulation results with two methods of RBF-MPC and RBF-ANFIS-MPC.

Method	Initial SOC	Final SOC	Fuel (L/100 km)	Calculation Time (s)
RBF-MPC	60	61.26	17.16	0.034
RBF-ANFIS-MPC	60	60.51	16.11	0.026

As shown in Figure 19, the SOC maintenance effect of the method of RBF-ANFIS-MPC is better in the global cycle condition. As can be seen in Figure 20, the energy management strategy based on RBF-ANFIS-MPC has lower fuel consumption. As shown in Table 4, compared with the RBF-MPC energy management strategy, the RBF-ANFIS-MPC energy management strategy has a smaller calculation cost, the average calculation time is reduced from 0.034 s to 0.026 s, and the final SOC value is closer to the initial SOC value, which is 60.51%. In addition, the simulation results show that on this basis, the vehicle fuel economy was also improved, with the final fuel consumption reduced from 17.16 L to 16.11 L.

5. Conclusions

This paper presented an energy management strategy with an ANFIS-based optimization of time horizon length, using distributed electric drive hybrid heavy-duty vehicles as

the research object. First, the velocity prediction model based on an RBF neural network is used to predict the future velocity sequence. After that, ANFIS was used to optimize and update the length of the forecast time horizon based on the predicted vehicle velocity sequence. Finally, compared with the fixed time horizon energy management strategy, which is based on MPC, the average calculation time of the energy management strategy is reduced by about 23.5%, and the fuel consumption per 100 km is reduced by about 6.12%.

When the vehicle is under different driving conditions, although the vehicle velocity error predicted by the prediction model in the prediction time horizon length leads to an error in the future vehicle velocity sequence, when the prediction time horizon length is short, if the power allocation calculation is carried out based on a fixed time horizon length, the power allocation results of the diesel genset and the power battery obtained are not the local optimal solution. Through simulation, it is obtained that appropriately increasing the prediction time horizon length can still reduce the vehicle fuel consumption, even if there is a situation of the accuracy of the vehicle horizon prediction result being reduced. It can not only further improve the local optimal performance of the energy management strategy but also improve the average calculation efficiency to achieve the global optimum.

Author Contributions: Data curation, T.L.; conceptualization, F.F.; project administration, C.W.; writing original draft, B.L. All authors have read and agreed to the published version of the manuscript.

Funding: This research is supported by the Natural Science Foundation of Beijing Province (Grant No. 4242047).

Data Availability Statement: The data that support the findings of this study are available from the corresponding author upon reasonable request.

Conflicts of Interest: Author Tao Liu was employed by the Inner Mongolia First Machinery Group Co., Ltd. The remaining authors declare that the research was conducted in the absence of any commercial or financial relationships that could be construed as a potential conflict of interest.

References

1. Yang, C.; Du, X.; Wang, W.; Yang, L.; Zha, M. A Rolling Convergent Equivalent Consumption Minimization Strategy for Plug-in Hybrid Electric Vehicles. *IEEE Trans. Veh. Technol.* **2024**, *73*, 3340–3353. [[CrossRef](#)]
2. Tang, X.; Jia, T.; Hu, X.; Huang, Y.; Deng, Z.; Pu, H. Naturalistic Data-Driven Predictive Energy Management for Plug-In Hybrid Electric Vehicles. *IEEE Trans. Transp. Electrification*. **2021**, *7*, 497–508. [[CrossRef](#)]
3. Biswas, A.; Emadi, A. Energy Management Systems for Electrified Powertrains: State-of-the-Art Review and Future Trends. *IEEE Trans. Veh. Technol.* **2019**, *68*, 6453–6467. [[CrossRef](#)]
4. Nguyen, N.-D.; Yoon, C.; Lee, Y.I. A Standalone Energy Management System of Battery/Supercapacitor Hybrid Energy Storage System for Electric Vehicles Using Model Predictive Control. *IEEE Trans. Ind. Electron.* **2023**, *70*, 5104–5114. [[CrossRef](#)]
5. Chatterjee, D.; Biswas, P.K.; Sain, C.; Roy, A.; Ahmad, F. Efficient Energy Management Strategy for Fuel Cell Hybrid Electric Vehicles Using Classifier Fusion Technique. *IEEE Access* **2023**, *11*, 97135–97146. [[CrossRef](#)]
6. Chang, C.; Fan, Z.; Wang, Z.; Liu, H. Research on Adaptive Two-Point Energy Management Strategy and Optimization for Range-Extended Electric Vehicle. *IEEE Access* **2023**, *11*, 90201–90213. [[CrossRef](#)]
7. Jia, C.; Qiao, W.; Cui, J.; Qu, L. Adaptive Model-Predictive-Control-Based Real-Time Energy Management of Fuel Cell Hybrid Electric Vehicles. *IEEE Trans. Power Electron.* **2023**, *38*, 2681–2694. [[CrossRef](#)]
8. Banvait, H.; Anwar, S.; Chen, Y. A rule-based energy management strategy for Plug-in Hybrid Electric Vehicle (PHEV). In Proceedings of the 2009 American Control Conference, St. Louis, MO, USA, 10–12 June 2009; pp. 3938–3943.
9. Li, Q.; Chen, W.; Li, Y.; Liu, S.; Huang, J. Energy management strategy for fuel cell/battery/ultracapacitor hybrid vehicle based on fuzzy logic. *Int. J. Electr. Power Energy Syst.* **2012**, *43*, 514–525. [[CrossRef](#)]
10. Zhou, S.; Chen, Z.; Huang, D.; Lin, T. Model prediction and Rule Based energy management strategy for a plug-in hybrid electric vehicle with hybrid energy storage system. *IEEE Trans. Power Electron.* **2021**, *36*, 5926–5940. [[CrossRef](#)]
11. Tao, F.; Zhu, L.; Ji, B.; Si, P.; Fu, Z. Energy management strategy using equivalent consumption minimization strategy for hybrid electric vehicles. *Secur. Commun. Netw.* **2020**, *2020*, 6642304. [[CrossRef](#)]
12. Li, J.; Wu, X.D.; Xu, M.; Liu, Y.G. A real-time optimization energy management of range extended electric vehicles for battery lifetime and energy consumption. *J. Power Sources* **2021**, *498*, 229939. [[CrossRef](#)]
13. Wieczorek, M.; Lewandowski, M. A mathematical representation of an energy management strategy for hybrid energy storage system in electric vehicle and real time optimization using a genetic algorithm. *Appl. Energy* **2017**, *192*, 222–233. [[CrossRef](#)]
14. Li, P.; Li, Y.; Wang, Y.; Jiao, X. An Intelligent Logic Rule-Based Energy Management Strategy for Power-Split Plug-in Hybrid Electric Vehicle. In Proceedings of the 2018 37th Chinese Control Conference (CCC), Wuhan, China, 25–27 July 2018; pp. 7668–7672.

15. Tao, F.; Zhu, L.; Fu, Z.; Si, P.; Sun, L. Frequency Decoupling-Based Energy Management Strategy for Fuel Cell/Battery/Ultracapacitor Hybrid Vehicle Using Fuzzy Control Method. *IEEE Access* **2020**, *8*, 166491–166502. [[CrossRef](#)]
16. Erdinc, O.; Vural, B.; Uzunoglu, M. A wavelet-fuzzy Logic Based energy management strategy for a fuel cell/battery/ultra-capacitor hybrid vehicular power system. *J. Power Sources* **2009**, *194*, 38–44. [[CrossRef](#)]
17. Hamlat, A.; Sekkour, M.; Mankour, M.; Khalfaoui, M. An improved energy management system for fuel cell/ultra-capacitor electric vehicle based fuzzy logic control. In *Artificial Intelligence and Heuristics for Smart Energy Efficiency in Smart Cities*; Springer: Cham, Switzerland, 2021; Volume 361, pp. 183–189.
18. Li, L.; Yang, C.; Zhang, Y.; Zhang, L.; Song, J. Correctional DP-Based Energy Management Strategy of Plug-In Hybrid Electric Bus for City-Bus Route. *IEEE Trans. Veh. Technol.* **2015**, *64*, 2792–2803. [[CrossRef](#)]
19. Peng, J.; He, H.; Xiong, R. Rule based energy management strategy for a series-parallel plug-in hybrid electric bus optimized by dynamic programming. *Appl. Energy* **2016**, *185*, 1633–1643. [[CrossRef](#)]
20. Zou, Y.; Hou, S.; Han, E.; Liu, L.; Chen, R. Dynamic Programming-based Energy Management Strategy Optimization for Hybrid Electric Commercial Vehicle. *Automot. Eng.* **2012**, *34*, 663–668.
21. Fan, L.; Wang, Y.; Wei, H.; Zhang, Y.; Zheng, P.; Huang, T.; Li, W. A GA-based online real-time optimized energy management strategy for plug-in hybrid electric vehicles. *Energy* **2021**, *241*, 122811. [[CrossRef](#)]
22. Ding, N.; Prasad, K.; Lie, T.T. Design of a hybrid energy management system using designed rule-based control strategy and genetic algorithm for the series-parallel plug-in hybrid electric. *Int. J. Energy Res.* **2021**, *45*, 1627–1644. [[CrossRef](#)]
23. Yuan, H.B.; Zou, W.J.; Jung, S.; Kim, Y.B. Optimized rule-based energy management for a polymer electrolyte membrane fuel cell/battery hybrid power system using a genetic algorithm. *Int. J. Hydrogen Energy* **2021**, *47*, 7932–7948. [[CrossRef](#)]
24. Tian, X.; He, R.; Sun, X.; Cai, Y.; Xu, Y. An ANFIS-Based ECMS for Energy Optimization of Parallel Hybrid Electric Bus. *IEEE Trans. Veh. Technol.* **2020**, *69*, 1473–1483. [[CrossRef](#)]
25. Rezaei, A.; Burl, J.B.; Zhou, B.; Rezaei, M. A New Real-Time Optimal Energy Management Strategy for Parallel Hybrid Electric Vehicles. *IEEE Trans. Control Syst. Technol.* **2019**, *27*, 830–837. [[CrossRef](#)]
26. Zhou, B.; Burl, J.B.; Rezaei, A. Equivalent Consumption Minimization Strategy with Consideration of Battery Aging for Parallel Hybrid Electric Vehicles. *IEEE Access* **2020**, *8*, 204770–204781. [[CrossRef](#)]
27. Zhou, Y.; Ravey, A.; Péra, M.-C. Multi-mode predictive energy management for fuel cell hybrid electric vehicles using Markov driving pattern recognizer. *Appl. Energy* **2019**, *258*, 114057. [[CrossRef](#)]
28. Li, T.; Liu, H.; Wang, H.; Yao, Y. Hierarchical predictive control-based economic energy management for fuel cell hybrid construction vehicles. *Energy* **2020**, *198*, 117327. [[CrossRef](#)]
29. Xie, S.; Hu, X.; Qi, S.; Tang, X.; Lang, K.; Xin, Z.; Brighton, J. Model predictive energy management for plug-in hybrid electric vehicles considering optimal battery depth of discharge. *Energy* **2019**, *173*, 667–678. [[CrossRef](#)]
30. Hao, J.; Ruan, S.; Wang, W. Model Predictive Control Based Energy Management Strategy of Series Hybrid Electric Vehicles Considering Driving Pattern Recognition. *Electronics* **2023**, *12*, 1418. [[CrossRef](#)]
31. Xiang, C.; Ding, F.; Wang, W.; He, W. Energy management of a dual-mode power-split hybrid electric vehicle based on velocity prediction and nonlinear model predictive control. *Appl. Energy* **2016**, *181*, 640–653. [[CrossRef](#)]
32. Kohut, N.J.; Hedrick, J.K.; Borrelli, F. Integrating Traffic Data and Model Predictive Control to Improve Fuel Economy. *IFAC Proc. Vol.* **2009**, *42*, 155–160. [[CrossRef](#)]
33. Yu, K.; Xu, X.; Hu, Z. Predictive control strategies for energy saving of hybrid electric vehicles based on traffic light information. *J. Hebei Univ. Sci. Technol.* **2015**, *36*, 480–486.
34. Shu, H.; Nie, T.; Deng, L.; Qiao, J. Model predictive control for a plug-in hybrid electric vehicle. *J. Chongqing Univ.* **2011**, *34*, 36–41.
35. Zhang, J.; Shen, T. Real-Time Fuel Economy Optimization with Nonlinear MPC for PHEVs. *IEEE Trans. Control Syst. Technol.* **2016**, *24*, 2167–2175. [[CrossRef](#)]
36. Hosseini, S.M.; Carli, R.; Dotoli, M. Robust Optimal Demand Response of Energy-efficient Commercial Buildings. In Proceedings of the European Control Conference (ECC), London, UK, 12–15 July 2022; pp. 1–6.
37. Lu, L.; Zhao, H.; Liu, X.; Sun, C.; Zhang, X.; Yang, H. MPC-ECMS Energy Management of Extended-Range Vehicles Based on LSTM Multi-Signal Speed Prediction. *Electronics* **2023**, *12*, 2642. [[CrossRef](#)]
38. Xu, E.; Ma, M.; Zheng, W.; Huang, Q. An Energy Management Strategy for Fuel-Cell Hybrid Commercial Vehicles Based on Adaptive Model Prediction. *Sustainability* **2023**, *15*, 7915. [[CrossRef](#)]
39. Liu, C.; Li, X.; Chen, Y.; Wei, C.; Liu, X.; Li, K. Real-time energy management strategy for fuel cell/battery vehicle based on speed prediction DP solver model predictive control. *J. Energy Storage* **2023**, *73*, 109288. [[CrossRef](#)]
40. Liu, J.; Liang, Y.; Chen, Z.; Yang, H. An ECMS Based on Model Prediction Control for Series Hybrid Electric Mine Trucks. *Energies* **2023**, *16*, 3942. [[CrossRef](#)]
41. Yang, X.P.; Jiang, C.Y.; Zhou, M.; Hu, H. Bi-level energy management strategy for power-split plug-in hybrid electric vehicles: A reinforcement learning approach for prediction and control. *Front. Energy Res.* **2023**, *11*, 1153390. [[CrossRef](#)]
42. Yao, Z.Y.; Shao, R.P.; Zhan, S.N.; Mo, R.; Wu, Z. Energy management strategy for fuel cell hybrid electric vehicles using Pontryagin’s minimum principle and dynamic SoC planning. *Energy Sources Part A-Recovery Util. Environ. Eff.* **2023**, *46*, 5112–5132. [[CrossRef](#)]
43. Chen, Z.; Gu, H.; Shen, S.; Shen, J. Energy management strategy for power-split plug-in hybrid electric vehicle based on MPC and double Q-learning. *Energy* **2022**, *245*, 123182. [[CrossRef](#)]

44. Cao, J.; Peng, J.; He, H. Research on Model Prediction Energy Management Strategy with Variable Horizon. *Energy Procedia* **2017**, *105*, 3565–3570. [[CrossRef](#)]
45. Kong, Y.; Xu, N.; Liu, Q.; Sui, Y.; Jia, Y. Variable horizon-based predictive energy management strategy for plug-in hybrid electric vehicles and determination of a suitable predictive horizon. *Energy* **2024**, *294*, 130809. [[CrossRef](#)]
46. Gillespie, T.D. *Fundamentals of Vehicle Dynamics*, 1st ed.; Tsinghua University Press: Beijing, China, 2006.
47. Bo, L.; Han, L.; Xiang, C.; Liu, H.; Ma, T. A Q-learning fuzzy inference system based online energy management strategy for off-road hybrid electric vehicles. *Energy* **2022**, *252*, 123976. [[CrossRef](#)]
48. Badreddine, B.; Amar, B.; Noureddine, H. Design and real-time implementation of an adaptive fast terminal synergetic controller based on dual RBF neural networks for voltage control of DC–DC step-down converter. *Electr. Eng.* **2022**, *104*, 945–957.
49. Jang, J.-S.R. ANFIS: Adaptive-network-based fuzzy inference system. *IEEE Trans. Syst. Man Cybern.* **1993**, *23*, 665–685. [[CrossRef](#)]
50. Djukanovic, M.B.; Calovic, M.S.; Vesovic, B.V.; Sobajic, D.J. Neuro-fuzzy controller of low head hydropower plants using adaptive-network based fuzzy inference system. *IEEE Trans. Energy Convers.* **1997**, *12*, 375–381. [[CrossRef](#)]
51. Kaloop, M.R.; Bardhan, A.; Kardani, N.; Samui, P.; Hu, J.W.; Ramzy, A. Novel application of adaptive swarm intelligence techniques coupled with adaptive network-based fuzzy inference system in predicting photovoltaic power. *Renew. Sustain. Energy Rev.* **2021**, *148*, 111315. [[CrossRef](#)]
52. Niasar, A.H.; Vahedi, A.; Moghbelli, H. ANFIS-based controller with fuzzy supervisory learning for speed control of 4-switch inverter brushless DC motor drive. In Proceedings of the 37th IEEE Power Electronics Specialists Conference, Jeju, Republic of Korea, 18–22 June 2006; pp. 1–5.

Disclaimer/Publisher’s Note: The statements, opinions and data contained in all publications are solely those of the individual author(s) and contributor(s) and not of MDPI and/or the editor(s). MDPI and/or the editor(s) disclaim responsibility for any injury to people or property resulting from any ideas, methods, instructions or products referred to in the content.